ADVANCED MATERIALS INTERFACES
www.advmatinterfaces.de

Bubble Control, Levitation, and Manipulation Using Dielectrophoresis

Carl V. Brown, Andrew M. J. Edwards, Abigail Roberts, Michael I. Newton, Ian C. Sage, Rodrigo Ledesma-Aguilar, and Glen McHale*

Bubbles attached to surfaces are ubiquitous in nature and in industry. However, bubbles are problematic in important technologies, including causing damage to the operation of microfluidic devices and being parasitic during heat transfer processes, so considerable efforts have been made to develop mechanical and electrical methods to remove bubbles from surfaces. In this work, liquid dielectrophoresis is used to force a captive air bubble to detach away from an inverted solid surface and, crucially, the detached bubble is then held stationary in place below the surface at a distance controlled by the voltage. In this "levitated" state, the bubble is separated from the surface by liquid layer with a voltage-selected thickness at which the dielectrophoresis force exactly counterbalances the gravitational buoyancy force. The techniques described here provide exceptional command over repeatable cycles of bubble detachment, levitation, and reattachment. A theoretical analysis is presented that explains the observed detachment–reattachment hysteresis in which bubble levitation is maintained with voltages in an order of magnitude lower than those used to create detachment. The precision surface bubble removal and control concepts are relevant to situations such as nucleate boiling and microgravity environments and offer an approach toward "wall-less" bubble microfluidic devices.

1. Introduction

In microfluidic systems, undesirable bubbles can often be nucleated inside the microchannels, or inadvertently introduced when connecting tubes. The motivation to develop techniques to promote bubble detachment from the surfaces in such systems, and subsequently transport the bubbles, is to avoid bubbles blocking the flow of liquid and/or amplifying the shear wall stress.[1,2] Such effects can limit the flow rate range that can be used, and even cause complete device failure.[3,4] In pool boiling-based heat exchanger devices bubbles become nucleated on the hot surfaces as the liquid begins to boil.[5] If allowed to persist and coalesce, dry patches can be formed which dramatically reduce the heat flux coming from the surface. Promoting bubble detachment in nucleate boiling is hence desirable, both to avoid such dry patches, as well to promote convective mixing to improve the overall heat flux.[6] This is particularly important for a microgravity environment where convection may be hindered and where buoyancy no longer aids detachment of nucleated bubbles.[7] A number of different methods have been developed to manage air bubbles within such systems. Passive mechanical mechanisms typically provide management of already free bubbles, rather than actively dislodging sessile or captive bubbles.[8] Electrical mechanisms, including high electric fields across the liquid, can promote bubble generation and have been shown to enhance nucleate boiling heat transfer.[9,10]

Electrowetting on dielectric (EWOD) is a technique which allows the reversable modification of the solid-liquid contact angle, θ of liquid droplets via a voltage applied between a conducting liquid at a surface and an electrode buried beneath a solid dielectric layer on that surface.[11–14] EWOD has become popular in applications such as optofluidics,[12] microfluidics,[15] and thermal management.[16,17] While the main body of work on EWOD focuses on decreasing the droplet contact angle by applied electric fields, the ability to detach sessile droplets from solid surfaces both in air and in a surrounding liquid medium has been demonstrated.[18,19] For example, detachment is promoted by partially spreading the liquid using EWOD, then allowing rapid recoiling to overcome the surface adhesion forces and promote droplet detachment.[20] 3D manipulation of liquid bubbles in a surrounding oil medium has been shown to be possible with bubbles being transferred from one surface to another via buoyancy.[20,21] EWOD has additionally been used to create bubble driven microfluidic devices,[22,23] and to detach air and liquid bubbles from a surface,[24,25] including

Prof. C. V. Brown, Dr. A. M. J. Edwards, A. Roberts, Dr. M. I. Newton, Dr. I. C. Sage
SOFT Group
School of Science and Technology
Nottingham Trent University
Clifton Lane, Nottingham NG11 8NS, UK
E-mail: carl.brown@ntu.ac.uk
Dr. R. Ledesma-Aguilar, Prof. G. McHale
Smart Materials and Surfaces Laboratory
Department of Mathematics
Physics and Electrical Engineering
Northumbria University
Ellison Place, Newcastle upon Tyne NE1 8ST, UK
The ORCID identification number(s) for the author(s) of this article can be found under https://doi.org/10.1002/admi.202001204.

DOI: 10.1002/admi.202001204

through the displacement of the air-liquid interface.[26] While EWOD approaches have shown the ability to detach pinned bubbles, key issues were highlighted such as requiring direct electrical contact with the liquid, working only with electrically conducting liquids, not providing any precise control over the bubble once it has become detached, and devices only removing bubbles on the first actuation.[24,26]

An alternative approach to reversibly modifying the wetting behavior of a liquid on a solid surface is dielectrowetting, which utilizes interface-localized liquid dielectrophoresis.[27,28] In this approach, dielectric liquid sessile droplets are deposited on a solid dielectric layer that over-coats interdigitated electrodes. By application of an A.C. voltage V_0 between interposing electrode fingers, a non-uniform electric field localized at the surface is generated which decays away from the surface exponentially characterized by a decay length, δ. The non-uniform electric field exerts a bulk force on the polarizable liquid which draws the liquid toward the region of highest electric field intensity.[29,30] Since the liquid is substantially more polarizable than vapor, surface-localized dielectrophoresis forces increase the area of the liquid-solid interface at the expense of the "dry" vapor-solid contact area which leads to a decreasing liquid droplet contact angle with increasing applied voltage. Dielectrowetting has been shown to promote reversible full film spreading and super-spreading overcoming the contact angle saturation present in EWOD.[28,31] Dielectrowetting has also found applications in a variety of optofluidic devices,[32] microfluidics,[33] and in improving heat transfer.[34]

In this work we demonstrate how dielectrophoresis can be used not only to force bubble detachment, but crucially, to promote a state of voltage-controlled levitation where a captive bubble can be held indefinitely away from a solid surface with programmable separation distance down to the micrometer scale. We elucidate how localized electric field gradients at the surface both force the reduction in vapor-solid contact area leading to detachment, and then counterbalance buoyancy to maintain a state of levitation for single and multiple bubbles (Movies M1 and M2†, Supporting Information). Furthermore, we show that at low voltages the same or other bubbles can be prevented from attaching or reattaching to the surface, even when a rising bubble meets the surface at speed or when mechanical force is applied to the bubble (Movies M3 and M4†, Supporting Information). Lastly, we demonstrate that our bubble levitation technique is equally applicable to both insulating liquids and to de-ionised water.

2. Results and Discussion

2.1. Dielectrophoresis Controlled Bubble Detachment, Levitation, and Reattachment

We pattern glass surfaces with a titanium-gold interdigitated microstripe electrode array capped with a thin planarizing dielectric layer and liquid-repellent coating of Teflon AF (Experimental and Methods Section). As the equilibrium Young's law contact angle of a sessile droplet of the dielectric liquid, trimethylolpropane triglycidyl ether (TMP-TG-E) on our Teflon coated surface is given by $\theta_Y = 82° \pm 1°$,[35,36] TMP-TG-E would not spontaneously form a stable thin wetting film on our surface.[37,38] The patterned glass surfaces were inverted and submersed in liquid TMP-TG-E and air bubbles were then created and attached to the solid surface by a needle. Once the bubble is attached, a three-phase contact line forms around the perimeter of the base of the captive bubble which encloses a circular "dry" vapor-solid base area, **Figure 1**a. The bubble contact angle is given at equilibrium by $\theta_e = \pi - \theta_Y = 98° \pm 1°$, measured from inside the bubble.

When a voltage is applied between the interdigitated electrodes the surface-localized dielectrophoretic forces cause

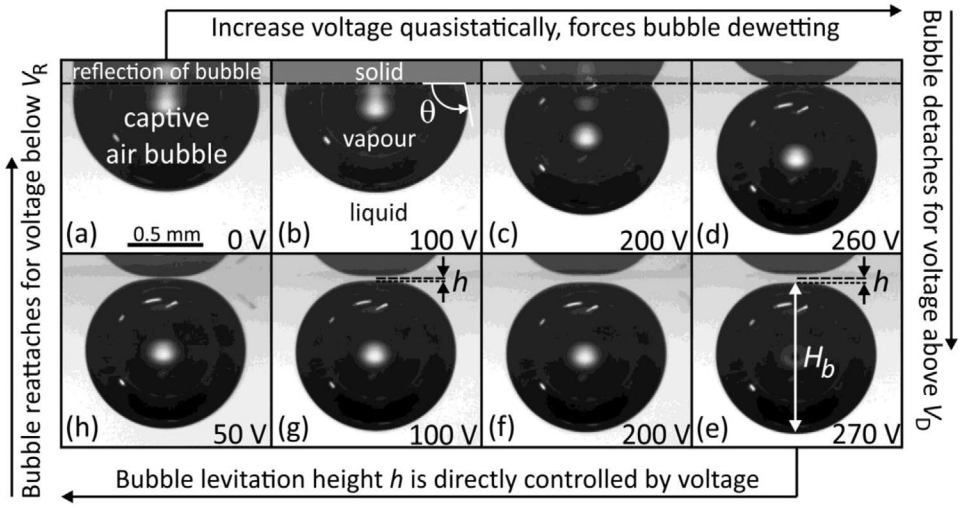

Figure 1. Experimental images demonstrating how dielectrophoresis force provide voltage-controlled bubble "dewetting" and detachment, levitation, and reattachment in the dielectric liquid TMP-TG-E. a) Image of a captive air bubble attached to an inverted solid surface immersed in the dielectric liquid. b–d) Increase in bubble contact angle upon application of a voltage, V_0 between interdigital microelectrodes buried within the surface. e) Detachment of the air bubble from surface at detachment voltage, V_D and static levitation below a stable voltage-controlled intervening liquid layer of thickness, h. f–h) Effect of changing V_0 on the thickness of the intervening liquid layer for a levitated bubble, with reattachment of the bubble back on to the surface at voltage V_R where $V_R \ll V_D$ demonstrating detachment–reattachment hysteresis. (Experimental parameters: liquid TMP-TG-E; bubble volume $\Omega = 0.51$ μL; electrode linewidth $l_e = 20$ μm).

increased wetting of the dielectric liquid, i.e., dielectrowetting, increasing the area of the solid-liquid interface, while reducing the vapor-solid area in the base of the bubble which is accompanied by a concomitant increase in the bubble contact angle, $\theta(V_0)$, as shown in Figure 1b–d. During the dewetting process, we find the vapor-solid area at the base of the bubble exhibits a small deviation from a circular shape, and this deviation is more pronounced for the largest bubble sizes in our study at high applied voltages (see Figure S1 in the Supporting Information). At a critical detachment voltage, V_D, the contact angle reaches $\theta = 180°$ and the dielectric liquid fully wets the surface, which detaches the bubble from the surface, Figure 1d,e. While bubbles can be detached in this manner via dielectrowetting for any orientation of the solid surface, if the surface is immersed in an inverted orientation liquid dielectrophoretic forces can counterbalance the buoyancy forces that would otherwise drive bubbles to attach to the surface, i.e., forcing a state of bubble levitation on an intervening liquid layer of thickness h. This situation is shown in the image in Figure 1e for an electrode voltage of $V_0 = 270$ V, which is slightly higher than the critical detachment voltage, $V_D = 269 \pm 1$ V. The thickness of the intervening liquid film in the gap between the bubble and the surface, h, varies monotonically as a function of the value of V_0, as shown in Figure 1e–h, and Movie M1† in the Supporting Information. As the value of V_0 is reduced below a threshold value, the reattachment voltage, V_R (here $V_R = 30 \pm 5$ V), then $h \to 0$ and the bubble reattaches back onto the surface, with a small gap shown in Figure 1h and then subsequent reattachment to produce a captive air bubble again, Figure 1a. There was no limit to the number of repeatable detachment, levitation, reattachment cycles that could be achieved.

It is remarkable that the reattachment voltage V_R is almost an order of magnitude lower than the detachment voltage V_D so detachment–reattachment hysteresis is exhibited for the system shown in Figure 1. Hence even low voltages are sufficient to prevent bubbles from attaching to the surface and, furthermore, at low voltages the same or other bubbles can be prevented from attaching or reattaching to the surface. This is demonstrated in Movie M3† in the Supporting Information where a fast rising bubble is prevented from attaching to a surface, and in Movie M4† in the Supporting Information where even a bubble that is mechanically squeezed to attempt to force it onto the surface is unable to attach to the surface, in both cases due to the surface-localized dielectrophoretic forces prevent bubble attachment while the voltage is applied.

2.2. Theoretical Analysis of the Attachment–Reattachment Hysteresis

We now develop an analytical model to describe the voltage dependence of surface-localized dielectrophoresis driven bubble "dewetting" and detachment $\theta(V_0)$, the subsequent suspended bubble vertical position control $h(V_0)$, and which will further provide insight into the origin of the detachment–reattachment hysteresis. An illustration of the forces acting on a levitated bubble is shown in **Figure 2**a. A detailed description of the mathematical model and the key assumptions made is provided in File F1† in the Supporting Information. Let the inverted solid surface be placed at position $z = 0$ in the x, y plane. Co-planar interdigitated microstripe electrodes with electrode linewidth, l_e equal to the inter-electrode gap l_g, are formed on this surface (see Figure 2b,c). An applied A.C. voltage of frequency f is applied between the electrode fingers, which we model as a simplified potential with a sinusoidal spatial dependence, where the angular frequency is $\omega = 2\pi/f$ and the spatial frequency is $k = \pi/2l_e = \pi/2l_g$. The electrodes are covered by a solid dielectric protection layer having thickness z_d and dielectric constant ε_d.

The solid dielectric is covered by a layer of thickness l_1 and dielectric constant ε_1, which is in turn covered by further layer having thickness l_2 and dielectric constant ε_2. Below these layers lies the oil reservoir. Our geometry, in which we are exponentially decaying strong electric field gradients localized to the surface, is hence very different from the normal electric field destabilization of spontaneously wetting liquid film described by Schäffer et al.[39,40] The general form of the electric potential in each of the regions of the system described above can be written in the form shown in Equation (1)

$$V(x,z,t) = \sqrt{2}\left(\frac{V_0}{2}\right)\sin\omega t\cos kx\left(\alpha e^{-kz} + \beta e^{kx}\right) \tag{1}$$

The non-uniform electric field produced by this potential, which has both normal and tangential in-plane spatially varying

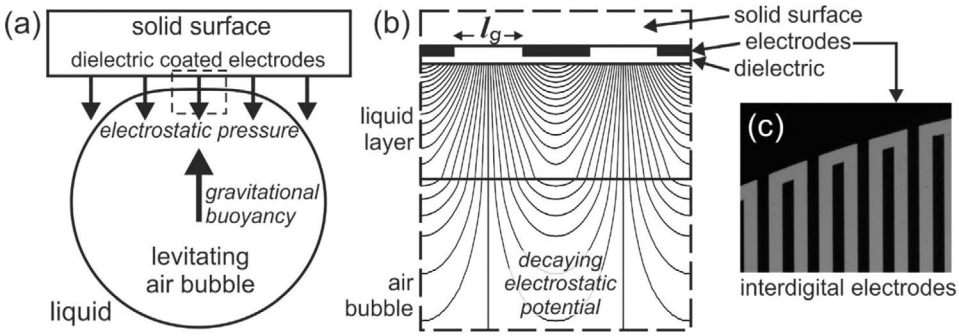

Figure 2. a) Illustration of the system showing the origin of the forces acting on a levitated air bubble that we model using Equations (2a) and (6). b) Zoom-in of the dashed region of a) showing the thin liquid film between the levitated air bubble and solid surface and interdigitated electrodes embedded in the dielectric layer. The decaying electrostatic potential is also shown. c) Top-down microscope image of the edge of the interdigital electrodes used in the device.

periodic components, is responsible both for generating and stabilizing the liquid film intervening between the bubble and the surface for bubble "dewetting" and the voltage control of bubble position, respectively.

The electric energy density at any position in the system is given by $1/2D \cdot E$ per unit volume, where $E = -\nabla V$ is the electric field, and $D = \varepsilon E$ is the displacement field. The electrostatic energy can be calculated using Equation (1) by applying appropriate electrostatic continuity conditions at the boundaries between the different regions, and integrating the electric energy density over a time period of the applied A.C. voltage, and over space for one period of the potential at the surface and from $z = 0$ to $z = \infty$. In the limits where $l_1 \gg l_e$ and $l_2 \gg l_e$, the electrostatic energy per unit surface area, W_e of the solid surface for this 3-layer system is given, to leading order, by Equation (2)

$$W_e = \frac{1}{8}\ \varepsilon_o \varepsilon_d k V_0^2 \left(a + be^{-2kh}\right) \tag{2a}$$

$$a = \frac{1}{2}\ \frac{\left[\varepsilon_1 \cosh kz_d + \varepsilon_d \sinh kz_d\right]}{\left[\varepsilon_d \cosh kz_d + \varepsilon_1 \sinh kz_d\right]} \tag{2b}$$

$$b' = -\frac{\varepsilon_d \varepsilon_1 (\varepsilon_1 - \varepsilon_2)}{(\varepsilon_1 + \varepsilon_2)[\varepsilon_d \cosh kz_d + \varepsilon_1 \sinh kz_d]^2} \tag{2c}$$

where, ε_0 is the permittivity of free space. First, we consider the electric field gradient forced bubble "dewetting" case corresponding to the experimental results shown in the images in Figure 1a–d. Equation (2) can be applied to this situation by assuming only a 2-layer system in which the solid dielectric is covered either by vapor or else by liquid, and so $\varepsilon_1 = \varepsilon_2$, $l_1 \to \infty$ and $b = 0$. Inside the base of the attached bubble the vapour is in contact with the solid dielectric surface, and so the electrostatic energy is given by Equation (2) with $\varepsilon_1 = \varepsilon_V$ and the expression for the coefficient in Equation (2b) will be denoted by a_V. It will be assumed that the height of the bubble is large and that the entire region above the solid dielectric is effectively filled with vapor. Outside the base of the attached bubble the liquid is in contact with the solid dielectric surface, and so the electrostatic energy is given by Equation (2) with $\varepsilon_1 = \varepsilon_L$ and the expression for the coefficient in Equation (2b) will be denoted by a_L. It will be assumed that for all values of the contact angle $\theta(V_0)$ the liquid layer is thick, so that the entire region above the solid dielectric is effectively filled with liquid.

Consider a sessile bubble on an activated interdigitated electrode array after a voltage-driven small change in the position of the contact line around the perimeter of the base of the bubble, resulting in a change ΔA in the bubble base area. Adding the electrostatic energy, Equation (2), to the unbalanced interfacial tension energies at the contact line provides the surface localized dielectrophoresis modified form of the change in the energy ΔW as a function in the change in bubble base area, Equation (3)

$$\Delta W \approx \Delta A \gamma_{LV}\left[\cos\left(\theta(V_0)\right) - \cos(\theta_e)\right] + \frac{1}{8}\Delta A \varepsilon_o \varepsilon_d\ k V_0^2 (a_L - a_V) \tag{3}$$

Here θ_e is the equilibrium contact angle inside the bubble, which is related to the Young's law angle θ_Y,[35,36] by $\theta_e = \pi - \theta_Y$ radians as discussed in Section 2.1, γ_{LV} is the surface energy of the liquid-vapor interface, and k is the spatial frequency, $k = \pi/2l_e = \pi/2l_g$. The equilibrium situation can be found by setting $\Delta W/\Delta A = 0$, which yields a surface localised dielectrophoresis modified version of Young's law for bubble "dewetting", Equation (4)

$$\cos\left(\theta(V_0)\right) = \cos(\theta_e) - \frac{\left(\varepsilon_o \varepsilon_d k (a_L - a_V)\right)}{8\gamma_{LV}} V_0^2 \tag{4}$$

where, $\theta(V_0)$ is the voltage dependent contact angle of the bubble and V_0 is the applied voltage at the electrodes. By substituting $\theta = 180°$ into Equation (4) an analytical expression for the critical detachment voltage V_D can be derived, given in Equation (5)

$$V_D = 2\sqrt{\frac{2\gamma_{LV}\left[1 - \cos(\theta_e)\right]}{\varepsilon_o \varepsilon_d k (a_L - a_V)}} \tag{5}$$

Equation (5) for the detachment voltage V_D, a ratio of surface tension and interfacial energy parameters in the numerator over dielectric terms in the denominator, expresses how the voltage induced polarization of the liquid adjacent to the surface needs to be sufficient to overcome surface energy forces to produce bubble detachment. **Figure 3**a shows how the value of the bubble contact angle $\theta(V_0)$ increases as the voltage V_0 is quasi-statically incremented. Up until $V_0 = 100$ V the contact angle does not change significantly because the dielectrophoresis force is insufficient to overcome contact line pinning effects. For voltages of 100 V and above the value of the contact angle increases monotonically and super linearly as a function of voltage V_0. The solid line in Figure 3a shows the fitting to Equation (4) (see Figure S3 in the Supporting Information). Hence we predict and experimentally observe the same $\cos\theta \propto V_0^2$ relationship for our liquid dielectrophoresis controlled bubble "dewetting" technique that has also previously also been found both for liquid EWOD,[11–14] and for liquid dielectrowetting.[28] This relationship may be used to extrapolate from the data to predict an experimentally derived value for the critical detachment voltage V_D at which the bubble contact angle would reach $\theta = 180°$. This is shown on Figure 3a by the vertical dashed line at $V_0 = V_D = 269 \pm 1$ V. Above this voltage, the greyed area in Figure 3a, the bubble is detached and enters the levitating state as shown in Figure 1e.

Next, we turn our attention to the voltage control of the vertical position of a suspended bubble, corresponding to the images in Figure 1e–h. Once the bubble has detached the surface is covered by an intervening liquid film layer with thickness $z_1 = h(V_0)$ and dielectric constant $\varepsilon_1 = \varepsilon_L$. The suspended bubble has a vertical height $z_2 = H_b$ and dielectric constant $\varepsilon_2 = \varepsilon_V$. The gravitational potential energy associated with the buoyancy of the bubble relative to the surface is given by Equation (6) below, where $\Delta\rho$ is the density difference between the liquid and air and g is the acceleration due to gravity

$$W_g = \Delta\rho g H_b \left(h(V_0) + \frac{H_b}{2}\right) \tag{6}$$

The total energy of the system is described by the sum of the gravitational potential energy associated with the buoyancy of the bubble, W_g Equation (6), and the electrostatic energy, W_e

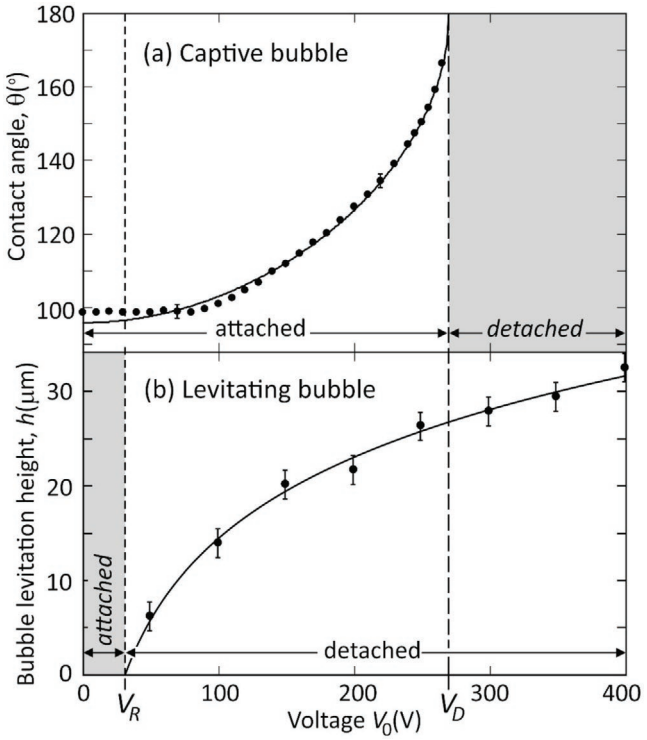

Figure 3. Hysteresis of the detachment, voltage-controlled levitation, and reattachment cycle. a) Change in bubble contact angle, $\theta(V_0)$ as a function of the applied voltage, V_0 for a bubble attached to the surface. Above at $V_D = 269 \pm 1$ V the bubble is detached from the surface. The solid line shows the fitting to Equation (4). b) Change in height of the bubble, $h(V_0)$ when levitated by the applied voltage, V_0. Below V_R the bubble reattaches to the surface. The solid line shows fitting to Equation (7). (Experimental parameters: liquid TMP-TG-E; bubble volume Ω = 0.51 μL; electrode linewidth l_e = 20 μm).

Equation (2). Minimizing the energy yields an expression for the equilibrium liquid film thickness $h(V_0)$ given in Equation (7)

$$h(V_0) = \frac{2l_e}{\pi} \log_e\left(\frac{V_0}{V_R}\right) \tag{7}$$

Where the reattachment voltage, V_R, is given in Equation (8)

$$V_R = 2\sqrt{\frac{2\Delta\rho g H_b l_e}{\varepsilon_o \varepsilon_d k\pi b'}} \tag{8}$$

Equation (8) for the reattachment voltage V_R, a ratio dominated by gravity related parameters in the numerator over dielectric terms dominating the denominator, expresses how the bubble can only reattach when the buoyancy then overcomes the polarization of the liquid film in place between the bubble and the surface when the voltage is reduced. Figure 3b shows how $h(V_0)$ decreases monotonically as the voltage V_0 is quasi-statically reduced where the solid line shows the fitting to Equation (7) (see Figure S3 in the Supporting Information). By extrapolation we are able to predict the experimentally derived value for the critical "touchdown voltage" V_R at which the thickness becomes zero, i.e., $h(V_R) = 0$ when $V_R = 30 \pm 5$ V. At, and below, this reattachment voltage V_R the electrostatic forces are no longer sufficient to counterbalance the buoyancy force which then pushes the bubble to reattach back onto the surface, the greyed area on Figure 3b. The reattachment mechanism that we have observed is that the liquid film punctures as the gap between the top of the bubble and the surface reduces toward zero.

Our theoretical model has successfully described the analytical voltage dependence of surface-localized dielectrophoresis driven bubble "dewetting" and detachment $\theta(V_0)$, the subsequent suspended bubble vertical position control $h(V_0)$. However, the measured and predicted numerical values of V_D, and of V_R, are not in quantitative agreement. The detachment voltage from the theory (Equation (5)) over-predicts the experimental value, V_D (theory) = 355 V compared with $V_D = 269 \pm 1$ V from extrapolation of the $\cos\theta \propto V_0^2$ fit to the experimental data shown in Figure 3a, and the reattachment voltage (Equation (8)) is under predicted, with V_R (theory) = 11 V compared with the value $V_R = 30 \pm 5$ V obtained by extrapolation from a $h \propto \log_e V_0$ fit to the experimental data shown in Figure 3b. These differences can be attributed to small deviations away from ideal circular base area during dewetting (see Figure S1 in the Supporting Information) and the sinusoidal potential function approximation that we used to describe the periodic surface potential produced by microstripe co-planar electrodes at $z = 0$, which is more complex in reality.[41,42] A complete theoretical treatment of the voltage control of bubble position would require numerical solution of the 3D electric fields in the system and the Maxwell and LaPlace contributions to the vapor-liquid interfacial stress,[43,36,44] to account for a non-spherical bubble shape and for the periodic deformation of the liquid film surface as thickness $h \to 0$.[45] Furthermore, we have used a flat liquid-vapor interface at the underside of the bubble, while the curved surface shape of the bubble and voltage induced periodic deformation of the liquid film surface will influence the actual reattachment voltage.

Our theory also provides meaningful insight into the detachment–reattachment hysteresis, notwithstanding these approximations, because we have retained the key geometrical and material parameter dependences of the system. An expression for the ratio of the detachment voltage to the reattachment voltage, $V_D/V_R \approx 3.5\Lambda_C/\sqrt{H_b l_e}$, where $\Lambda_C = \sqrt{\gamma_{LV}/\Delta\rho g}$ is the capillary length for the liquid, is found by making the approximations $z_d \to 0$, cos $(\theta) \approx -1$, and $\varepsilon_L \gg \varepsilon_V$. Hence, the key determining factor of the relative magnitudes of V_D and V_R is the comparison between the capillary length of the liquid, and the geometric mean of two key length-scales; the bubble vertical height, H_b and the electrode linewidth l_e. In our experiments depicted in Figure 1, $\Lambda_C \approx 2 \times 10^{-3}$ m, $H_b \approx 1.5 \times 10^{-3}$ m, and $l_e = 20 \times 10^{-6}$ m, and so V_D is over an order of magnitude larger than V_R and we observe significant hysteresis. So for a centimeter scale bubble on electrodes with millimeter linewidth the detachment–reattachment hysteresis would disappear, although both voltages would significantly increase, and if $V_R \geq V_D$ electrostatic bubble detachment would not be possible.

2.3. Dielectrophoresis Controlled Levitation—Key Parameter Dependencies

Figure 4 (and Movie M2†, Supporting Information) demonstrates simultaneous on-demand dielectrophoresis controlled

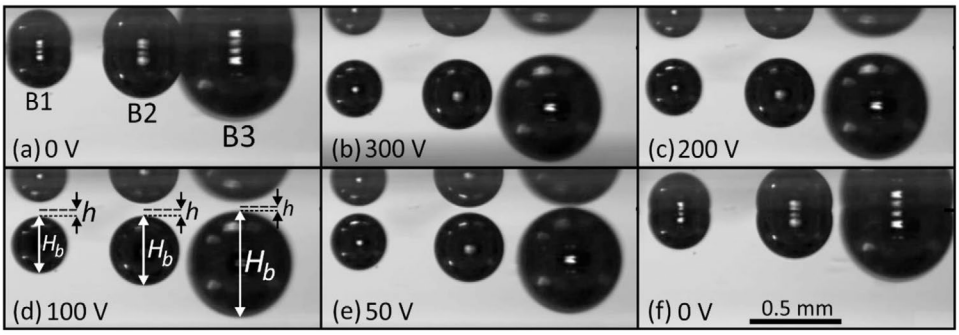

Figure 4. Experimental images showing the simultaneous detachment, voltage-controlled levitation, and reattachment of three separate bubbles that have different volumes. a) Attached bubbles at 0 V. b–e) Voltage-controlled levitation at various heights, demonstrating how the bubble height, H_b affects the separation distance, $h(V_0)$ for a given applied voltage, V_0. f) Reattachment at 0 V. (Experimental parameters: liquid TMP-TG-E; electrode linewidth $l_e = 40$ μm).

bubble detachment, levitation and reattachment of multiple bubbles with different volumes. Repeated and reproducible cycling between detachment and reattachment at the region of the inverted surface is demonstrated. In the detached levitated state, as discussed above, the bubble is separated from the surface by liquid layer with a voltage-selected thickness at which the dielectrophoresis force exactly counterbalances the gravitational buoyancy force, and the latter depends on the vertical height and volume of a bubble. Hence, for a given constant voltage V_0, larger bubbles will be held suspended at a smaller levitation height $h(V_0)$. This is demonstrated in Figure 4d, where the largest levitation height is exhibited for the bubble on the left that has the smallest vertical height H_b (and smallest volume Ω), compared to the smallest levitation height which is exhibited for the bubble on the right that has the largest vertical height H_b.

Figure 5 shows the results of dielectrophoresis bubble levitation control experiments for seven different bubbles. This detailed study provides data for a ranges of voltages V_0 in each case, and for two different dielectric liquids (TMP-TG-E with ε_L = 13.7, and propylene glycol PG with ε_L = 35), two different electrode linewidths (l_e = 20 and 40 μm), and multiple bubble volumes (in the range over two decades, Ω = 0.015 μL to Ω = 3.46 μL). The levitation height $h(V_0)$ is plotted against $(2l_e/\pi)\log_e(V_0/V_R)$, where the value of V_R is separately experimentally determined for each data set. We find that all of the data is well represented by a common unity gradient, shown by the solid line on the graph in Figure 5. Hence we observe that the gradient of h versus $\log_e(V_0/V_R)$ shows linear dependence on only one parameter, the linewidth l_e of the interdigitated microelectrodes that are buried within the surface. The gradient is found to be independent of the size of the bubble and independent of the dielectric constant of the liquids used in the system, in agreement with the prediction of Equation (7).

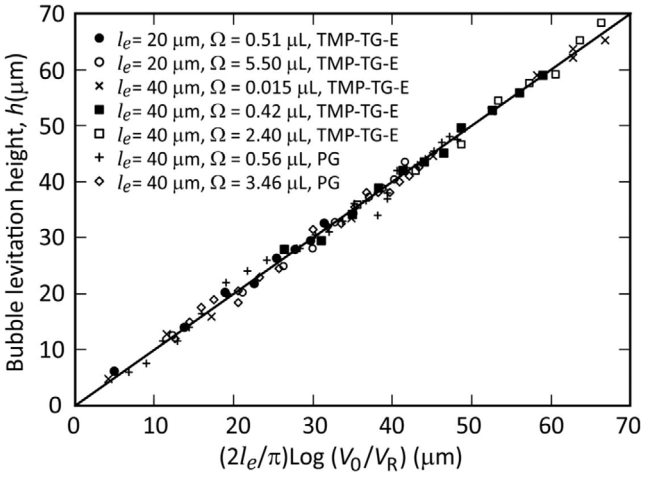

Figure 5. Comparison of the bubble levitation height h against $2l_e/\pi$ log(V_0/V_R) for 7 experimental datasets covering two dielectric liquids (TMP-TG-E and Propylene glycol, PG), two electrode linewidths (l_e = 20 μm and l_e = 40 μm) and multiple bubble volumes (Ω = 0.015 μL to Ω = 3.46 μL). The solid line, which has a gradient of unity, is a guide to the eye.

2.4. Future Prospects for Further Development of Our Levitation Concepts

Once the bubbles are in the voltage-controlled levitation state we find that they are constrained to remain within the electrode boundary, as shown in Movie M5† in the Supporting Information. As a levitated bubble approaches the edge of the underlying electrode structure the bubble is repelled from the extremities of the structure leading to a lateral confinement of the bubble which is entirely electrically controlled. Once the applied voltage is removed the electrostatic potential barrier is also removed and the bubble can cross outside the electrode area. This indicates that guidance of levitated bubbles is possible in a "wall-less" configuration, where electrostatic potential barriers can be placed and removed at will to control bubble trajectories without any solid or moving parts.

While the focus of the current work has been on bubble detachment, levitation and reattachment in non-conducting dielectric liquids, our concepts are also applicable to conducting liquids. This is illustrated by the experiment shown in Movie M6† in the Supporting Information which shows the dielectrophoresis forced detachment, levitation with movement under gravity (the surface was not completely horizontal), and reattachment of an air bubble in de-ionized water with a conductivity of 1.7 μS m^{-1}. We also demonstrate

in de-ionized water the ability to prevent attachment of large approaching bubbles to the surface, due to the localized electric field gradient, and to vary the voltage to alter the separation distance of a large levitated bubble (Movies M7 and M8†, Supporting Information). Theoretical description of these results will require the development of models that include the effects of finite conductivity, which may be possible by extending the current model to include the polarization effects associated with lossy dielectrics in the case of relatively low conductivity liquid systems.

3. Conclusions and Discussion

In this work, we have shown how a vapor filled bubble can be "dewetted" and detached from a solid surface by dielectrowetting with an applied voltage V_D which exceeds a critical value. Once the bubble is free from an inverted surface, it enters a state of voltage-controlled levitation where changing the voltage allows precise, micrometer scale control over the separation distance. We further demonstrate how a localized electric field gradient prevents other approaching rising bubbles from attaching to the surface. For the system demonstrated here, the electrostatic pressure remains sufficient to maintain a stable liquid film, preventing bubble reattachment to the surface, even for voltages of a few tens of volts—almost an order of magnitude lower than the initial detachment voltage. At or below a critical touchdown voltage V_R puncturing of the intervening liquid film between the bubble and the surface occurs, precipitating the buoyancy driven reattachment of the bubble to the surface. Hence cycling the voltage to above the critical detachment voltage, and then to below the critical touchdown voltage, provides repeatable bubble detachment–reattachment control (Movies M1 and M2†, Supporting Information). Our theoretical model successfully describes the dependence of the contact angle during electric field gradient forced bubble "dewetting," and the dependence of the liquid film thickness on the voltage and the electrode linewidth during controlled levitation. The geometry of the system is shown to play a key role in determining the value of both the detachment and reattachment touchdown voltages. We have further demonstrated switchable "wall-less" voltage-controllable lateral confinement of levitated bubbles, potentially reducing the level of intricacy required for microfluidic devices. Finally, we have demonstrated that our concepts of dielectrophoresis controlled bubble detachment, levitation and reattachment apply equally to dielectric liquids and to conducting liquids.

We note how our dielectrophoresis controlled vapor filled bubble detachment and reverse "levitation" mirrors the Leidenfrost effect, which has previously been shown to levitate and transport liquid droplets on a vapor layer above a structured surfaces.[46,47] However, unlike Leidenfrost droplet transport where the direction is fixed by the structure of the solid surface, our vapor-filled bubble held detached below a surface by an electric field gradient stabilized liquid layer can be actuated on demand by using sets of interdigitated fingers which have a small overlap,[33] where by application of different voltages to the sets, a reprogrammable spatially varying h_0 can be created. This creates spatial variation of the magnitude of the electric field gradients in the plane of the surface which the bubble responds to due to buoyancy, hence permitting directional bubble actuation.

Hence the ability described in this work to electrostatically detach, i.e., to dislodge and control bubbles at will in dielectric and conducting liquids has potential applications in; improving efficiency by rapidly removing nucleated bubbles in immersion heat transfer,[48–50] as an active "debubbler" in conventional microfluidics, for controlling bubbles in microgravity environments,[7] as well as opening up new avenues to achieving "wall-less" surface driven bubble-microfluidics with the intervening liquid layer avoiding the issues associated with moving contact lines.[51]

4. Experimental Section

The experiments were carried out on air bubbles deposited onto solid surfaces immersed within one of two different dielectric liquids, trimethylolpropane triglycidyl ether (TMP-TG-E, CAS: 3454-29-3, dielectric constant, $\varepsilon = 13.7$, density, $\rho = 1160$ kg m^{-3}, surface tension $\gamma_{LV} = 44$ mJ m^{-2}) and propylene glycol (CAS: 57-55-7 dielectric constant, $\varepsilon = 35$, density, $\rho = 1040$ kg m^{-3}, surface tension, $\gamma_{LV} = 38.6$ mJ m^{-2}). Bubbles of volume in the range of 0.4–2.4 µL were created by injecting air onto the underside of the solid surface using a syringe. An array of interdigitated co-planar parallel microstripe electrodes fabricated from gold on titanium was patterned on the solid surface. The electrode linewidths equaled the electrode gaps, and two linewidths were used in the experiments, 20 and 40 µm. The surface and the electrodes were coated with a SU-8 dielectric layer (Microchem Corp., thickness 1 µm, dielectric constant 3.2) to prevent any conduction through the liquid. A final capping layer of Teflon AF was added to the device to promote retraction of the liquid from the surface, which imparted an equilibrium contact angle of 95° measured inside a bubble in TMP-TG-E, and 95° measured inside a bubble in PG. To coat the devices in Teflon AF, a solution was made from 0.5% w.t. of Poly[4,5-difluoro-2,2-bis(trifluoromethyl)-1,3-dioxole-co-tetrafluoroethylene] (CAS: 37626-13-4) in the solvent Octadecafluorodecahydronaphthalene (CAS: 306-94-5). Substrates were dip-coated in the solution, allowed to dry at room temperature before baking at 155 °C for 20 min to cure.

The localized electric field gradient at the solid surface was produced by applying a sinusoidal A.C. voltage (V_0) at 10 kHz to alternate fingers of an interdigitated microstripe electrode array within the solid surface, with the interposed electrode fingers at earth potential.

For the DI water experiments, an electrode linewidth and gap of 200 µm was used with a PDMS dielectric layer (Sylgard-184., thickness 12 µm) to prevent any conduction through the liquid.

Supporting Information

Supporting Information is available from the Wiley Online Library or from the author.

Acknowledgements

This work was supported by the U.K. Engineering and Physical Sciences Research Council (Grant Nos. EP/R036837/1 and EP/R042276/1).

Conflict of Interest

The authors declare no conflict of interest.

Keywords

bubbles, dewetting, liquid dielectrophoresis, surfaces, wetting

Received: July 6, 2020
Revised: August 28, 2020
Published online: September 28, 2020

[1] E. Leclerc, Y. Sakai, T. Fujii, *Biomed. Microdevices* **2003**, *5*, 109.
[2] C. Lochovsky, S. Yasotharan, A. Günther, *Lab Chip* **2012**, *12*, 595.
[3] D. D. Meng, J. Kim, C. J. Kim, *J. Micromech. Microeng.* **2006**, *16*, 419.
[4] J. H. Kang, Y. C. Kim, J. K. Park, *Lab Chip* **2008**, *8*, 176.
[5] C. Gerardi, J. Buongiorno, L. W. Hu, T. McKrell, *Int. J. Heat Mass Transfer* **2010**, *53*, 4185.
[6] J. Kim, *Int. J. Multiphase Flow* **2009**, *35*, 1067.
[7] M. Q. Raza, N. Kumar, R. Raj, *Sci. Rep.* **2016**, *6*, 19113.
[8] D. Cheng, H. Jiang, *Appl. Phys. Lett.* **2009**, *95*, 1.
[9] P. Cooper, *J. Heat Transfer* **1990**, *112*, 458.
[10] J. Ogata, A. Yabe, *Int. J. Heat Mass Transfer* **1993**, *36*, 775.
[11] B. Berge, *C.R Acad. Sci. Paris Ser II* **1993**, *317*, 157.
[12] B. Berge, J. Peseux, *Eur. Phys. J. E: Soft Matter Biol. Phys.* **2000**, *3*, 159.
[13] F. Mugele, J. C. Baret, *J. Phys.: Condens. Matter* **2005**, *17*, R705.
[14] F. Mugele, J. Heikenfeld, *Electrowetting Fundamental Principles and Practical Applications*, Wiley-VCH, Berlin **2019**.
[15] S. K. Cho, H. Moon, C. J. Kim, *J. Microelectromech. Syst.* **2003**, *12*, 70.
[16] J. T. Cheng, C. L. Chen, *Exp. Fluids* **2010**, *49*, 1349.
[17] J. T. Cheng, C. L. Chen, *Nanoscale Microscale Thermophys. Eng.* **2010**, *14*, 63.
[18] S. J. Lee, S. Lee, K. H. Kang, *J. Visualization* **2011**, *14*, 259.
[19] S. J. Lee, S. Lee, K. H. Kang, *Appl. Phys. Lett.* **2011**, *100*, 081604.
[20] S. J. Lee, J. Hong, K. H. Kang, I. S. Kang, S. J. Lee, *Langmuir* **2014**, *30*, 1805.
[21] J. Hong, Y. K. Kim, D. J. Won, J. Kim, S. J. Lee, *Sci. Rep.* **2015**, *5*, 10685.
[22] J. H. Lee, K. H. Lee, J. M. Won, K. Rhee, S. K. Chung, *Sens. Actuators, A* **2012**, *182*, 153.
[23] S. K. Chung, K. Rhee, S. K. Cho, *Int. J. Precis. Eng. Manuf.* **2010**, *11*, 991.
[24] S. Wang, H. H. Chen, C. L. Chen, *Appl. Phys. Lett.* **2016**, *108*, 181601.
[25] J. Hong, S. J. Lee, *Lab Chip* **2015**, *15*, 900.
[26] H. Xu, R. Yan, S. Wang, C. Chen, *Phys. Fluids* **2017**, *29*, 102105.
[27] C. V. Brown, G. G. Wells, M. I. Newton, G. McHale, *Nat. Photonics* **2009**, *3*, 403.
[28] G. McHale, C. V. Brown, M. I. Newton, G. G. Wells, N. Sampara, *Phys. Rev. Lett.* **2011**, *107*, 186101.
[29] H. A. Pohl, *Dielectrophoresis: The Behaviour of Neutral Matter in Non-Uniform Electric Fields Cambridge Monographs on Physics*, Cambridge University Press, Cambridge **1978**.
[30] T. B. Jones, M. Gunjii, M. Washizu, M. J. Feldman, *J. Appl. Phys.* **2001**, *89*, 1441.
[31] A. M. J. Edwards, C. V. Brown, M. I. Newton, G. McHale, *Curr. Opin. Colloid Interface Sci.* **2018**, *36*, 28.
[32] S. Xu, H. Ren, S. T. Wu, *J. Phys. D: Appl. Phys.* **2013**, *46*, 483001.
[33] H. Geng, J. Feng, L. M. Stabryla, S. K. Cho, *Lab Chip* **2017**, *17*, 1060.
[34] Y. Hyun, K. Y. Lee, S. Ko, S. K. Chung, in *IEEE 32nd Int. Conf. on Micro Electro Mechanical Systems (MEMS 2019)*, Institute of Electrical and Electronics Engineers (IEEE), Piscataway, NJ **2019**.
[35] A. W. Adamson, A. P. Gast, *Physical Chemistry of Surfaces*, Wiley, Chichester, NY **1997**.
[36] P. G. De Gennes, F. Brochard-Wyart, D. Quere, *Capillarity and Wetting Phenomena: Drops, Bubbles, Pearls, Waves*, Springer, New York **2004**.
[37] B. Saramago, *Curr. Opin. Colloid Interface Sci.* **2010**, *15*, 330.
[38] V. S. Ajaev, E. Y. Gatapova, O. A. Kabov, *Adv. Colloid Interface Sci.* **2016**, *228*, 92.
[39] E. Schäffer, T. Thurn-Albrechet, T. P. Russel, U. Steiner, *Nature* **2000**, *403*, 874.
[40] E. Schäffer, T. Thurn-Albrechet, T. P. Russel, U. Steiner, *Europhys. Lett.* **2001**, *53*, 518.
[41] X. Wang, X. B. Wang, F. F. Becker, P. R. C. Gascoyne, *J. Phys. D: Appl. Phys.* **1996**, *29*, 1649.
[42] M. W. Den Otter, *Sens. Actuators, A* **2002**, *96*, 140.
[43] L. D. Landau, E. M. Lifshitz, L. P. Pitaeveskii, *Electrodynamics of Continuous Media*, Pergamon Press, Oxford **1984**.
[44] D. T. Papageorgiou, *Annu. Rev. Fluid Mech.* **2019**, *51*, 155.
[45] C. V. Brown, G. McHale, N. J. Mottram, *J. Appl. Phys.* **2011**, *110*, 024107.
[46] J. G. Leidenfrost, *De aquae communis nonnullis qualitatibus tractatus*, Ovenius, Duisburg **1756**.
[47] H. Linke, B. J. Alemán, L. D. Melling, M. J. Taormina, M. J. Francis, C. C. Dow-Hydelund, V. Narayanan, R. P. Taylor, A. Stout, *Phys. Rev. Lett.* **2006**, *96*, 154502.
[48] V. K. Patel, J. Seyed-Yagoobi, *J. Heat Transfer* **2017**, *139*, 061502.
[49] A. Bar-Cohen, *JSME Int. J., Ser. B* **1993**, *36*, 1.
[50] R. C. Chu, R. E. Simons, M. J. Ellsworth, R. R. Schmidt, V. Cozzolino, *IEEE Trans. Device Mater. Reliab.* **2004**, *4*, 568.
[51] Y. Zhao, S. K. Cho, *Lab Chip* **2007**, *7*, 273.